Rapid and Robust Polyprotein Production Facilitates Single-Molecule Mechanical Characterization of β-Barrel Assembly Machinery Polypeptide Transport Associated Domains

Toni Hoffmann,[†,‡,§,∥] Katarzyna M. Tych,[†,‡,∥] Thomas Crosskey,[§] Bob Schiffrin,[‡,§] David J. Brockwell,[*,‡,§] and Lorna Dougan[*,†,‡]

[†]School of Physics and Astronomy, [‡]Astbury Centre for Structural and Molecular Biology, and [§]School of Molecular and Cellular Biology, University of Leeds, Leeds, LS2 9JT, U.K. [∥]T. Hoffmann and K. M. Tych contributed equally to this work.

ABSTRACT Single-molecule force spectroscopy by atomic force microscopy exploits the use of multimeric protein constructs, namely, polyproteins, to decrease the impact of nonspecific interactions, to improve data accumulation, and to allow the accommodation of benchmarking reference domains within the construct. However, methods to generate such constructs are either time- and labor-intensive or lack control over the length or the domain sequence of the obtained construct. Here, we describe an approach that addresses both of these shortcomings that uses Gibson assembly (GA) to generate a defined recombinant polyprotein rapidly using linker sequences. To demonstrate the feasibility of this approach, we used GA to make a polyprotein composed of alternating domains of I27 and *Tm*Csp, $(\text{I27-}TmCsp)_3\text{-I27})^{GA}$, and showed the mechanical fingerprint, mechanical strength, and pulling speed dependence are the same as an analogous polyprotein constructed using the classical approach. After this benchmarking, we exploited this approach to facilitiate the mechanical characterization of POTRA domain 2 of BamA from *E. coli* (*Ec*POTRA2) by assembling the polyprotein $(\text{I27-}EcPOTRA2)_3\text{-I27}^{GA}$. We show that, as predicted from the $\alpha + \beta$ topology, *Ec*POTRA2 domains are mechanically robust over a wide range of pulling speeds. Furthermore, we identify a clear correlation between mechanical robustness and brittleness for a range of other $\alpha + \beta$ proteins that contain the structural feature of proximal terminal β-strands in parallel geometry. We thus demonstrate that the GA approach is a powerful tool, as it circumvents the usual time- and labor-intensive polyprotein production process and allows for rapid production of new constructs for single-molecule studies. As shown for *Ec*POTRA2, this approach allows the exploration of the mechanical properties of a greater number of proteins and their variants. This improves our understanding of the relationship between structure and mechanical strength, increasing our ability to design proteins with tailored mechanical properties.

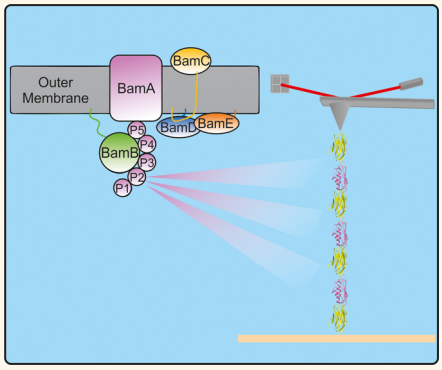

KEYWORDS: Gibson assembly · polyprotein · force spectroscopy · BamA (β barrel assembly machinery) · POTRA (polypeptide transport associated) · protein unfolding

Single-molecule force spectroscopy using the atomic force microscope (AFM) is an important technique to study the mechanical stability and energy landscape of single proteins by mechanically perturbing their structure.[1−7] Using this approach, protein molecules are immobilized on a surface, and the AFM probe is repeatedly brought into contact with the surface. Upon immobilization to the tip of the AFM cantilever, through a nonspecific interaction, the tethered protein is extended *via* retraction of the tip at a constant velocity[3] or by varying the tip−substrate separation to apply a constant force.[3] As both methods increase the distance between the surface and the cantilever tip, a mechanical force is exerted, and the protein is stretched, leading to successive domain unfolding, which finally results in a fully unfolded protein. While single-protein domains can be used,[8] polyprotein chains

* Address correspondence to L.Dougan@leeds.ac.uk, D.J.Brockwell@leeds.ac.uk.

Received for review April 1, 2015 and accepted August 18, 2015.

Published online August 18, 2015
10.1021/acsnano.5b01962

(which comprise repeats of identical or alternating protein domains) are typically employed.[3] These polyproteins provide clear mechanical fingerprints in single-molecule force spectroscopy experiments, such as the sawtooth pattern seen in force−extension traces collected in a constant-velocity experiment. The use of polyproteins is important, as it reduces the frequency of nonspecific interactions between the AFM probe and the surface relative to *bona fide* protein unfolding events and it increases the number of data points collected for a given approach and retraction cycle.[8] Polyproteins can consist either of identical protein domains, termed homopolyproteins, or of alternating domains of different proteins, termed chimeric or heteropolyproteins.[3]

A number of different techniques have been employed to engineer such polyproteins. A classical approach is based on the assembly of polymerase chain reaction (PCR)-generated DNA cassettes that together encode the full-length polyprotein.[3,9−11] This method uses specific restriction sites between DNA fragments that encode respective protein domains. Sequential enzymatic digestions and ligations generate the full-length polyprotein DNA in a stepwise manner.[3] This method allows for the precise control of the number of domains in the polyprotein and the order of protein domains within a chimeric polyprotein. This method has consequently been employed to make a wide range of different homo- and chimeric polyprotein constructs, making it a versatile method for polyprotein production.[12] However, in this approach the substitution of single DNA fragments occurs sequentially, making the process both laborious and time-intensive. Variants of this method such as ligating multiple copies of a single "cassette" encoding the nonpalindromic restriction site (*Ava*I) at its termini[10] or the iterative ligation of cassettes that encode *Bam*HI and *Bgl*II or *Nhe*I and *Spe*I restriction sites 5′ and 3′ to the gene[10,13−16] are quicker but yield less defined products or cannot be used to construct more complex polyproteins. An alternative method is based on the chemical coupling of identical protein monomers[17−24] or dimers[25,26] Here, proteins can be linked through either disulfide bridge formation between cysteine pairs at designed locations or maleimide coupling of sulfhydryl groups within the protein.[21,22,27−29] This chemical coupling allows for a faster one-step construction of polyproteins. It also has the advantage of allowing the study of different pulling directions by changing the position of linkage groups on the surface of the protein.[20] However, this method precludes the generation of more complex protein scaffolds and generates an ensemble of low- to high-order multimers, which may have an impact on the subsequent analysis of the experimental data.[30−32]

Here we apply a recently developed method (Gibson assembly (GA), Figure 1), which allows for rapid production of both homo- and heteropolyproteins of specific length and sequence, thereby retaining the benefits of the "cassette" approach described above (defined composition) while addressing its previous drawback (expense in terms of labor and time). The enzymatic assembly of DNA using GA[33] allows for the joining of many (up to 20) DNA fragments in a single step, using the combined function of three enzymes: a 5′ exonuclease, a DNA polymerase, and a DNA ligase. The application of GA to generate polyprotein open reading frames compared to previous methods is advantageous because it provides the speed and ease of a single-step chemical coupling of protein monomers while allowing for control over type, order of domains, and length of the designed polyprotein. Here, we describe the application of the GA method to generate polyproteins for use in force spectroscopy experiments. This involves a novel design of specific linker regions to join individual protein domains. Two different chimeric polyproteins were generated in this study. The first was (I27-*Tm*Csp)$_3$-I27, which contained four copies of the 27th immunoglobulin-like domain of human cardiac titin (I27) and three copies of the cold shock protein B domain from the hyperthermophilic organism *Thermotoga maritima* (*Tm*Csp). We have previously generated this polyprotein using the standard cassette method and characterized it using AFM.[34,35] The generation of the same construct using the GA method thus served as an important control to check the feasibility of this approach. The second construct was (I27-*Ec*POTRA2)$_3$-I27,

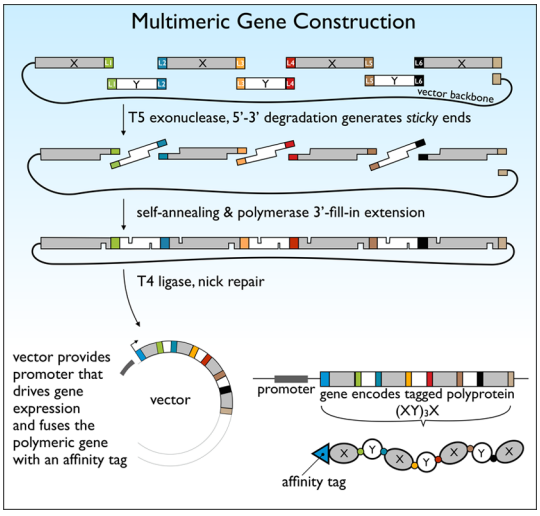

Figure 1. Gibson assembly (GA) cloning. The GA of a vector encoding a heptameric polyprotein requires the assembly of seven DNA modules. The process involves assembling a heptameric polyprotein open reading frame encoding two, interdigitated domains (X and Y) separated by short peptide linker sequences (colored rectangles). Amplified DNA PCR products that encode protein domains and the vector backbone and possess overlapping ends are mixed. T5 exonuclease degrades the DNA in the 5′−3′ direction and generates recessed, sticky ends. Self-annealing of compatible ends occurs while DNA polymerase fills in gaps. Finally, T4 ligase covalently joins DNA fragments to generate a fully assembled vector containing DNA encoding the chimeric polyprotein, (XY)$_3$-X.

which contained four I27 domains and three copies of the second polypeptide transport associated (POTRA) domain from the *Escherichia coli* outer membrane insertase protein BamA (*Ec*POTRA2).[36] This domain, a component of an essential bacterial complex,[37] has a mechanically uncharacterized fold but is topologically similar to several other proteins previously studied by single-molecule force methods.

RESULTS AND DISCUSSION

Polyprotein Construction by Gibson Assembly. GA cloning depends on the presence of compatible overhanging ends in the DNA "cassettes". As polyproteins used in force spectroscopy experiments consist of protein domains joined by unstructured peptide linkers, these regions can be used to encode complementary overlap regions between GA-compatible cassettes, allowing for the ordered assembly of DNA molecules. The recommended length for GA-compatible overhangs is 20 nucleotides.[33] Thus, we designed linker peptides made of seven amino acids encoded by 21 nucleotides guided by the following principles: (i) the linkers should have similar physicochemical properties at the protein level but be sufficiently distinct at the DNA level to allow specific and ordered assembly and (ii) the chosen amino acids should ensure steric freedom and minimize any potentially interfering interactions with neighboring protein domains. Figure 2A shows the sequence of each linker based on a symmetrical design with a central glycine (G) and a combination of uncharged, polar (S, serine; T, threonine) and nonpolar residues (A, alanine; I, isoleucine; L, leucine; V, valine). By shuffling these residues while keeping the location of the central glycine constant, six unique linker peptides emerged possessing a global palindromic-like symmetry while maintaining the same amino acid composition and length (Figure 2A). At the DNA level, the specificity of the complementary region at cassette termini was further increased by switching between the two most frequently used codons for each amino acid (Figure 2B). GA was carried out as described in the Methods section. Briefly, DNA cassettes that encode individual protein domains (Figure 1, where X designates the previously mechanically characterized I27 domain and Y the protein under study) as well as the linearized backbone containing the first I27 domain (Table 1, Supporting Information), were obtained by standard PCR methods and joined to form a circular DNA molecule by GA cloning. Full-length assembled constructs were identified by colony PCR, and their successful assembly was confirmed by DNA sequencing.

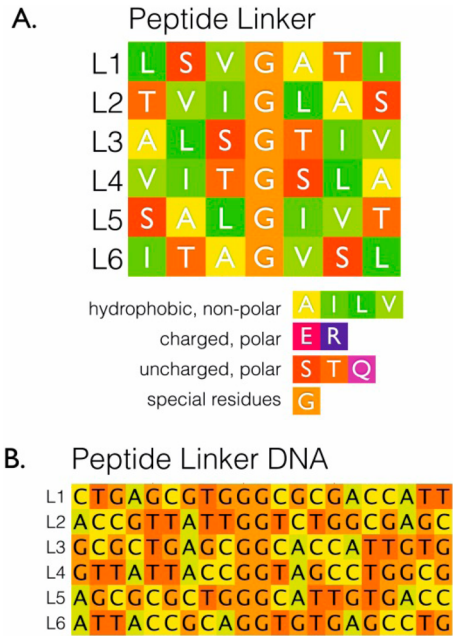

Figure 2. Peptide linker design. (A) GA-compatible linker peptides were designed comprising a balanced, symmetrical combination of seven polar and nonpolar uncharged residues. (B) Higher specificity between adjacent cassettes was achieved by switching between the two most frequently used codons for each amino acid in *E. coli*.

Reduction in Time for Polyprotein Engineering. Compared to standard cloning techniques, GA cloning reduces the time to obtain polyprotein samples that can be mechanically tested on an AFM. The process starts with the PCR-based amplification and purification of GA cloning compatible fragments followed by the GA reaction itself. On the same day, competent *E. coli* cells are transformed and spread onto selective plates. On day 2, positive clones are selected by colony PCR, and liquid overnight cultures are inoculated, allowing identification of successful constructs after only 3 days. To date, this method has been used to construct seven polyproteins-encoding plasmids. Of these plasmids, 13% (min = 4%, max = 35%) contained a fully assembled construct. By contrast to the rapidity of GA, the classical construction of polyproteins[3] takes significantly longer. First, a PCR-amplified DNA fragment is subcloned into a bacterial expression vector that contains a polyprotein construct (e.g., $(X)_7$), using restriction digestion of a unique pair of sites to replace the second protein domain encoding fragment in $(X)_7$, for example. This results in a X-Y-$(X)_5$ construct that needs to be selected by analytical digest/colony PCR and confirmed by sequencing. This will take a minimum of 6 days. Once confirmed, this construct is used for subsequent rounds of cloning to replace further DNA fragments (e.g., the fourth and the sixth domain), totaling about 18 days of experimental work before a full construct ($(X\text{-}Y)_3$-X) is confirmed. In reality, the subsequent repetitions of subcloning and selection increase the likelihood of failures and further delays.

Single-Molecule AFM Experiments on (I27-*Tm*Csp) Polyprotein Prepared by Gibson Assembly. To validate this approach, a polyprotein made by GA comprising alternating domains of the I27 and *Tm*Csp protein *Thermatoga maritima* was constructed (*Tm*Csp, $((I27\text{-}TmCsp)_3\text{-}I27)^{GA}$),

expressed, and purified. Its mechanical unfolding properties were then characterized by AFM (Figure S1) and compared to those of a homologous polyprotein constructed using the cassette approach ((I27-*Tm*Csp)$_3$-I27).[35] Full details of the sequences of both constructs can be found in the Supporting Information. The interpeak distance (x_{p2p}), defined as the distance from one unfolding peak to the same force value on the following curve, and the peak unfolding force (F_U) were then measured for each unfolding event, and frequency histograms were constructed for both x_{p2p} and F_U. Excellent agreement can be found for x_{p2p} and F_U values measured for the constructs made using each method (Supporting Information and Figure S1). We followed the same procedure to obtain force−extension traces at three other pulling velocities; 100, 200 (Figure S1), and 2000 nms^{-1} (Figure S2 and Table S2). At each pulling velocity we completed three experiments to measure F_U for each type of unfolding event and constructed three histograms of F_U. We found that the pulling speed dependence of F_U for *Tm*Csp and I27 were the same for both (I27-*Tm*Csp)$_3$-I27^{GA} and (I27-*Tm*Csp)$_3$-I27 (Figure S2, Table S2).

Investigating the Mechanical Strength of *Ec*POTRA2. Having benchmarked polyproteins constructed by GA against a homologous, previously characterized polyprotein, we employed this method to facilitate the rapid construction of a novel polyprotein that comprised I27 and a mechanically uncharacterized domain, the second POTRA domain of BamA (residues 92−173) from the *E. coli* BAM complex (*Ec*POTRA2). The function of BAM (β-barrel assembly machinery) is to fold and insert β-barrel outer membrane proteins (OMPs) into the outer membrane of Gram-negative bacteria, with homologous machinery present in mitochondria and chloroplasts (Figure 3).[37−39] BamA, which carries out OMP insertion by an as yet unknown mechanism, is essential for cell viability and comprises a β-barrel domain and five N-terminal, tandemly arrayed POTRA domains that extend into the periplasm.[40]

BamA POTRA domains are thought to perform three functions: (i) to act as a scaffold for complex formation; (ii) to interact with periplasmic chaperones, and (iii) to form a binding site for OMP substrates. The mechanism(s) by which POTRA domains facilitate OMP folding and insertion is unclear but may involve a scaffolding role (by β-sheet augmentation between POTRA β-strands and the nascent OMP)[41,42] or even a more active role by driving OMP β-hairpin formation by cycling between bent and extended conformations.[41] Single-molecule force unbinding studies[43,44] are ideally suited to address this question, but a prerequisite to such a study is the full characterization of the mechanical properties of the POTRA domains themselves. In addition to its function where mechanical scaffolding may play a role, *Ec*POTRA2 was also selected for study because it has an ideal topology to further our understanding of the relationship between protein structure, sequence, and mechanical strength of topologically simple proteins. Accordingly, this $\alpha+\beta$ domain is 81 residues in length and comprises a three-stranded β-sheet packed against two helices (β1-α1-α2-β2-β3), whose N- and C-termini are located on two neighboring parallel β-strands (Figure 3).[36,45] From a mechanical unfolding perspective this is an attractive topology, as these two strands might form a mechanical clamp region that conveys resistance to an applied force.[12,46,47]

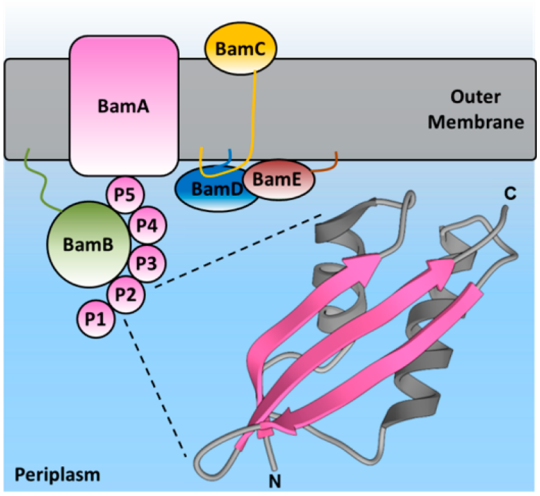

Figure 3. (A) Schematic of the BAM (β-barrel assembly machinery) complex in *E. coli*. The central component of the machinery is the outer membrane β-barrel protein BamA. The N-terminal periplasmic component of BamA consists of five POTRA domains (P1−P5). A ribbon representation of the tertiary structure for *Ec*POTRA2 is shown in the inset. In the AFM protein unfolding experiments *Ec*POTRA2 is extended from the amino- and carboxy-terminal ends (N and C).

Mechanically unfolding (I27-*Ec*POTRA2)$_3$-I27 revealed a sawtooth-like unfolding force−extension pattern corresponding to the sequential unfolding of single domains of either *Ec*POTRA2 or I27 (Figure 4A). While the interpeak distance (x_{p2p}) between each unfolding event appears similar (~22 nm), unfolding appears to occur at two distinct forces (~112 and 175 pN). A scatter plot (Figure 4C) that combines the data for x_{p2p} and F_U reveals two populations of events, one population at lower forces (highlighted by the pink-shaded region) and a second population at higher forces (highlighted by the yellow-shaded region). The latter distribution agrees well with the forces measured previously for I27 at this pulling speed (163 ± 15 pN).[34] The distribution of x_{p2p} values (highlighted by the yellow-shaded region) is similar and the median x_{p2p} value is in close agreement to that measured previously for I27 at this pulling speed (23.0 nm).[34] The shorter x_{p2p} distribution (highlighted by the pink-shaded region) reflects the slightly smaller size of the folded core of *Ec*POTRA2 relative to I27 (81 and 89 residues, respectively). These data thus demonstrate

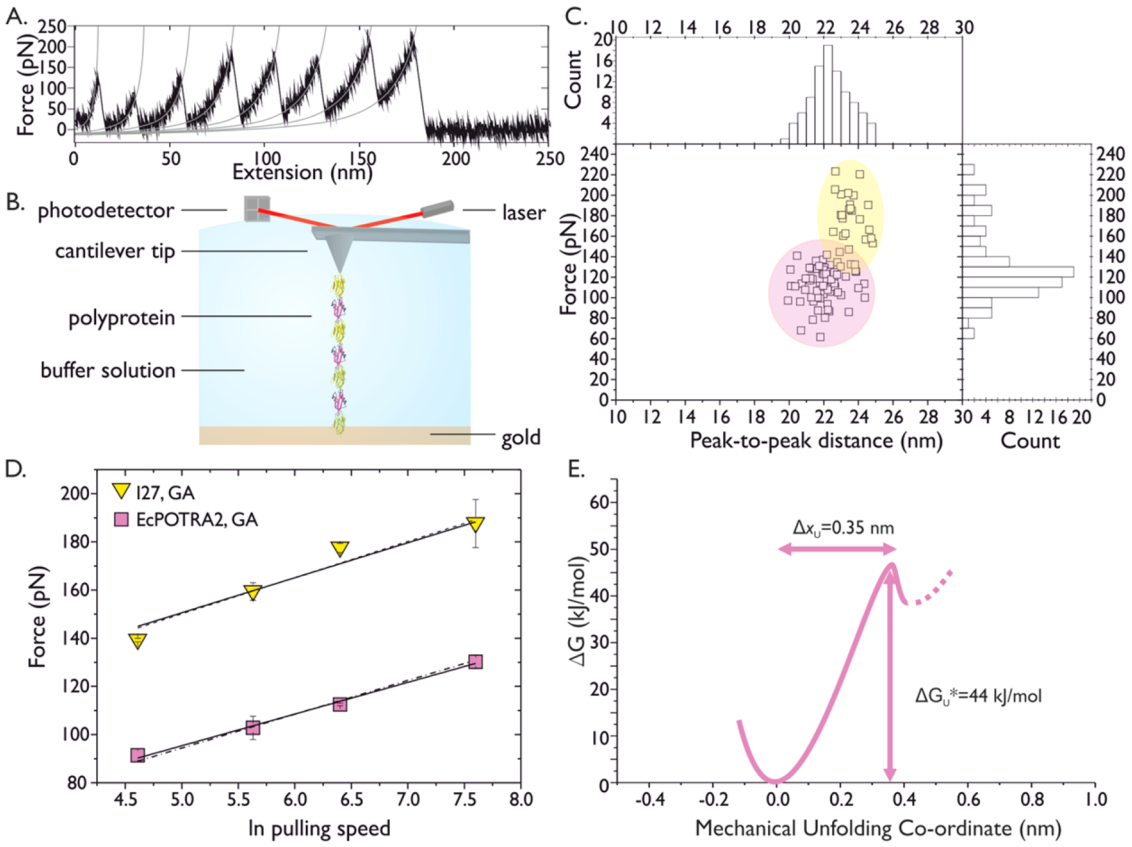

Figure 4. Investigating the mechanical properties of a POTRA domain. (A) Mechanical unfolding at a constant velocity of 600 nm s^{-1} of the (I27-*Ec*POTRA2)$_3$-I27 polyprotein constructed using GA. The worm-like chain (WLC) model fit to the data is shown in gray. (B) Schematic showing a single (I27-*Ec*POTRA2)$_3$-I27 molecule (*Ec*POTRA2 and I27, pink and yellow, respectively) attached to a gold surface (bottom) and the tip of an AFM cantilever (top). (C) The scatter plots of *Ec*POTRA2 (pink) and I27 (yellow) unfolding forces and interpeak distances for 96 unfolding events are shown as the same symbol with colored regions to indicate their separation based on the force histogram. (D) Pulling speed dependence of the mechanical unfolding of (I27-*Ec*POTRA2)$_3$-I27. The mechanical unfolding forces for *Ec*POTRA2 (pink squares) and I27 (yellow triangles) at 23 °C. Each pair of data points at a given pulling speed show the average of the Gaussian mean values of the unfolding force for *Ec*POTRA2 and I27 from three experiments completed under the same conditions. The error bars indicate the standard deviation between the three experiments. Solid lines are the best fit to the data. The Monte Carlo fits to the experimental data are shown as dashed lines. (E) Schematic of the unfolding energy landscape for *Ec*POTRA2 with parameters obtained using the Monte Carlo fits to experimental results. These include the activation energy barrier height (ΔG^*) and the distance from the native, folded state to the unfolding transition state (Δx_U).

that *Ec*POTRA2 exhibits significant mechanical stability and unfolds in a single step.

Unfolding Energy Landscape of *Ec*POTRA2. Force−extension traces at three other pulling velocities (100, 280, and 2000 nm s^{-1}) were obtained to assess the pulling speed dependence of *Ec*POTRA2. The F_U histograms at each speed and the statistics for each experiment can be found in the Supporting Information (Figure S3 and Table S3). Figure 4D shows that F_U for *Ec*POTRA2 (pink squares) and I27 (yellow triangles) both increase as a function of pulling speed. Parameters that describe the underlying unfolding energy landscapes of the proteins, namely, ΔG_U^*, the height of the activation energy barrier, and Δx_U, the distance between the folded state and the transition barrier on the mechanical unfolding pathway, were then obtained from this dependence using a Monte Carlo method.[34] For *Ec*POTRA2 we obtained $\Delta x_U = 0.35 \pm 0.01$ nm and $k_U = 0.0200 \pm 0.0020$ s^{-1} (dashed line, Figure 4D). Assuming a value of the prefactor[48] $A = 10^6$ s^{-1}, this gives an activation energy barrier height $\Delta G_U^* = 44$ kJ mol^{-1} for *Ec*POTRA2. Comparing this with I27, we obtained $\Delta x_U = 0.32 \pm 0.04$ nm, $k_U = 0.0013 \pm 0.0001$ s^{-1}, and $\Delta G_U^* = 45$ kJ mol^{-1}, in agreement with previous studies.[34,35] While the height of the activation energy barrier to unfolding is very similar for *Ec*POTRA2 and I27, the distance to the unfolding transition state is slightly larger for *Ec*POTRA2.

Mechanical Stability of α + β Proteins. The data set from protein mechanical unfolding experiments has greatly expanded in the past decade,[12] permitting understanding of the measured differences in protein mechanical strength. Previously we completed a review of all experimental data on single-molecule characterization of proteins using the AFM and showed that proteins that are mechanically strong and exhibit high unfolding forces are typically "brittle", with small Δx_U values.[12] Conversely, proteins that exhibit low

unfolding forces are typically "soft", with large Δx_U values. While β-strand-rich proteins populate the strong and brittle end of the spectrum, α-helical-rich proteins are comparatively weak and soft. An interesting intermediate region is populated by proteins that are α-helical and β-strand-rich, such as *Ec*POTRA2 studied here. An updated review of the current literature shows that experiments to measure the pulling speed dependence of the unfolding force, F_U (such as those shown in Figure 4D), has been completed for 11 other $\alpha + \beta$ proteins[16,49−57] (shown in Figure 5A). These include proteins such as the extensively studied ubiquitin, protein G, and protein L[52,53,58] as well as the more recently studied SUMO proteins.[57] The 12 $\alpha + \beta$ proteins range in size from 56 amino acids (protein G) to 155 amino acids (RNase H) and have varied α-helical and β-sheet content (Figure 5B). There is no correlation between the amount of α-helix or β-sheet content and F_U. Comparing the experimentally measured F_U at 600 nm s^{-1} and Δx_U for each of the 12 $\alpha + \beta$ proteins (Figure 5C) reveals a power law dependence (solid line, Figure 5C) of the form $\Delta x_U = 45.0/F_U$. The scaling law indicates that mechanically weaker $\alpha + \beta$ proteins have a larger value of Δx_U, indicative of a "softer" protein structure that can be deformed to a greater extent before reaching the unfolding transition state and unfolding. The power law dependence measured for $\alpha + \beta$ proteins (Figure 5C) is in agreement with previous work on a broader range of protein structures, including all-β proteins and all-α proteins.[12] Here, by focusing on a specific class of protein ($\alpha + \beta$) we can obtain a more accurate correlation between F_U and Δx_U, including an improved chi-squared value. Of the 12 $\alpha + \beta$ proteins studied to date, eight are mechanically strong (F_U > 100 pN at 600 nm s^{-1}) and relatively brittle (*i.e.*, small Δx_U < 0.51 nm), while four proteins are mechanically weak (F_U < 70 pN at 600 nm s^{-1}) and malleable (*i.e.*, large Δx_U > 0.68 nm). It is interesting to consider whether the mechanically strong and brittle proteins share any common features that the mechanically weak and malleable proteins lack. Inspection of the structure of the $\alpha + \beta$ proteins studied to date by AFM (Figure 5A) shows that six proteins possess directly adjacent N- and C-terminal β-strands in a parallel alignment (protein G, protein L, SUMO2, ubiquitin, *Ec*POTRA2, and SUMO1). This geometry has previously been hypothesized as the main reason for mechanical stability in β-strand-containing proteins, as proteins with this geometry at the termini have been found to have higher unfolding forces[14,51,52] than those

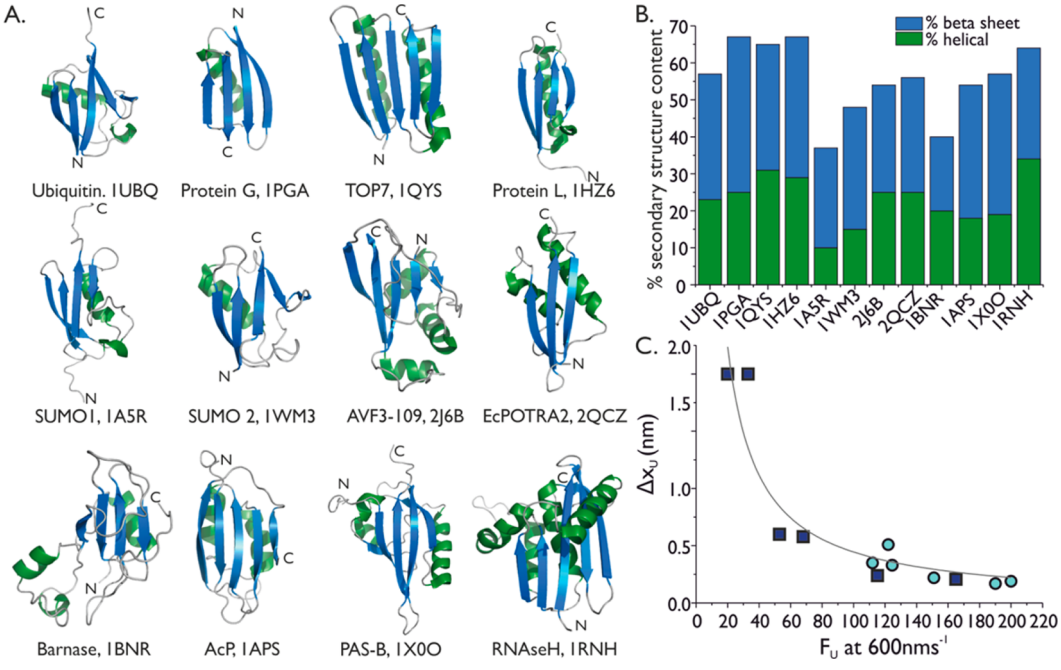

Figure 5. Mechanical stability of $\alpha + \beta$ proteins. (A) $\alpha + \beta$ proteins studied using single-molecule force spectroscopy using the AFM for which a pulling speed dependence of the mechanical stability has been obtained. Proteins are shown in ribbon representations with β-strands as blue arrows and α-helices as green ribbons. The proteins are extended from their amino- and carboxy-terminal ends (N and C). The relevant PDB accession code is shown for each protein. The proteins are ordered by their unfolding force F_U at 600 nm s^{-1}, with ubiquitin having the largest F_U and RNaseH the smallest F_U. (B) Histograms show the percentage of α-helical (green) and β-sheet (blue) content in each protein, calculated from the PDB structure. The proteins are again ordered by their unfolding force F_U at 600 nm s^{-1}. (C) Graph showing the unfolding force F_U at a pulling speed of 600 nm s^{-1} and the unfolding distance Δx_U for $\alpha + \beta$ proteins which have been experimentally unfolded at least at two different speeds. Where required, the expected unfolding force at 600 nm s^{-1} was interpolated. The data can be described by a bootstrapped, nonlinear fit following a power law with $\Delta x_U = 45.0 \pm 10.5/F_U$ ($R^2 = 0.86 \pm 0.01$). Examination of the structure of the 12 $\alpha + \beta$ proteins reveals a subset of proteins (blue circles) that possess a similar structural feature: directly connected, parallel alignment of the N- and C-terminal β-strands. $\alpha + \beta$ proteins that lack this structural feature are shown as dark blue squares.

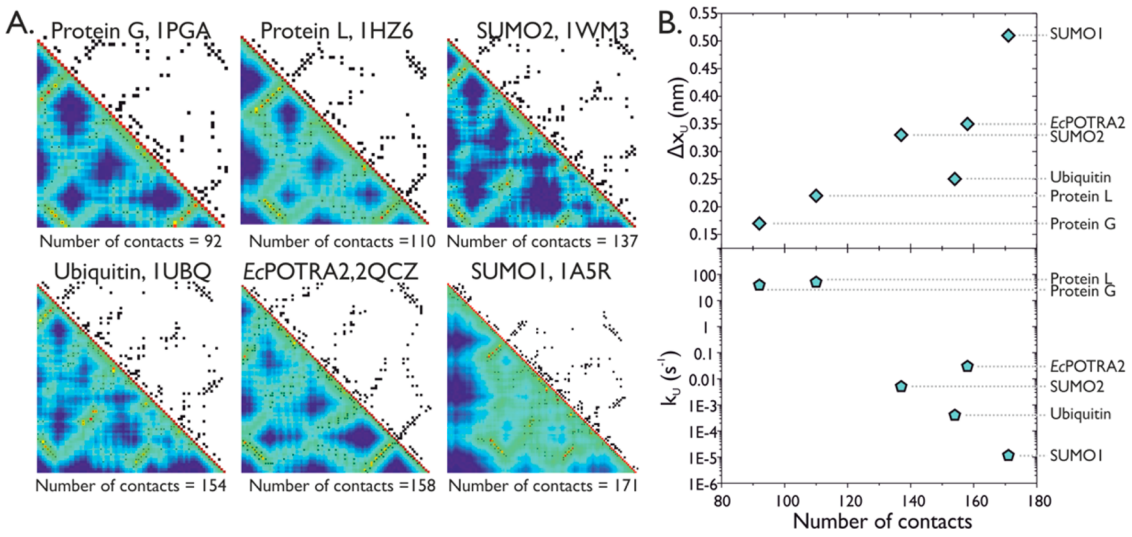

Figure 6. Number of inter-residue contacts correlates with Δx_U and k_U. (A) Contact maps for the six $\alpha + \beta$ proteins that have proximal terminal β-strands in parallel geometry: protein G, protein L, SUMO2, ubiquitin, *Ec*POTRA2, and SUMO1. The protein name is followed by its PDB accession code. An inter-residue contact was assumed to be present if the shortest distance between side-chain atoms of different residues was <5 Å. Distances above the distance cutoff are shown in blue, distances around the cutoff are shown in green, and distances below the cutoff are shown in red, where the darkest blue is the longest distance and the darkest red is the shortest distance. Distances are calculated between C-alpha atoms. In the black and white section, a contact between two residues is colored black if it is present according to the defined distance cutoff. (B) The number of inter-residue contacts correlates with Δx_U (upper) and with k_U (lower) for the six $\alpha + \beta$ proteins.

which lack this feature.[50] To understand further the mechanical properties of $\alpha + \beta$ proteins, we calculated the inter-residue contacts in the proteins that possess proximal, parallel β-strands at their termini and constructed contact maps for each protein (Figure 6A). An inter-residue contact was assumed to be present if the shortest distance between side-chain atoms of different residues was <5 Å, the same cutoff used in a similar study on SUMO proteins.[57] For the six identified $\alpha + \beta$ proteins we find that the number of contacts increases from 92 contacts in protein G to 171 in the SUMO1 protein. Interestingly, we find a clear correlation between both Δx_U and k_U and the number of contacts (Figure 6B), where the Δx_U and k_U from each study have been obtained using a similar method to that employed in the present study using *Ec*POTRA2. This correlation was not observed when all 12 of the $\alpha + \beta$ proteins that have been studied using single-molecule force spectroscopy are included (Figure S4). As the number of contacts increases for the six identified $\alpha + \beta$ proteins, Δx_U increases (Figure 6B, upper) and k_U decreases (Figure 6B, lower), resulting in enhanced malleability and mechanical stability. Possessing a large number of inter-residue contacts may be an important feature for mechanical stability, providing the protein with increased options for contacts breaking and re-forming elsewhere along the force-deformed structure as the force is applied. Such a property could be attractive in the formation of self-healing biomaterials where, under a mechanical stress, bonds can break and readily re-form.[59]

Previous studies on the unfolding processes of protein L, protein G, ubiquitin, and SUMO1 and 2 suggest that these proteins unfold by a similar structural mechanism.[16,51,57] The transition state to unfolding is thought to involve the breaking of contacts between two well-defined structural units. For example, for protein L one structural unit comprises β-strands I and II and the helix (light blue in protein L schematic Figure 7A), and the second unit involves the β-hairpin of strands III and IV (dark blue in protein L schematic Figure 7A). As the transition states to unfolding for several of the proteins described here are known to involve the breaking of contacts between two well-defined structural units,[51,57] we divided each of the six $\alpha + \beta$ proteins identified into two structural units (shown as light blue and dark blue in Figure 7A). Contacts between these two structural units were defined as interfacial contacts. We examined the contact maps of side-chain contacts (nearest distance between atoms of two residues <5 Å) using CMView software[60] and found that there is a correlation between the number of interfacial contacts and the measured Δx_U (upper) and with k_U (lower) for five of the $\alpha + \beta$ proteins (Figure 7B). For example, protein G has only 26 contacts and a relatively small Δx_U, while EcPOTRA2 has 50 contacts and a relatively large Δx_U. The higher number of long-range contacts between mechanically important structural units may be the cause of the higher mechanical resilience in *Ec*POTRA2, as these residues must first be broken apart before the protein can be extended.

The exception is SUMO 1, which has 42 contacts and a higher Δx_U (Figure 7B, upper) than the other five $\alpha + \beta$ proteins, which have proximal terminal β-strands in parallel geometry. To examine this further, we calculated the number of inter-residue hydrogen

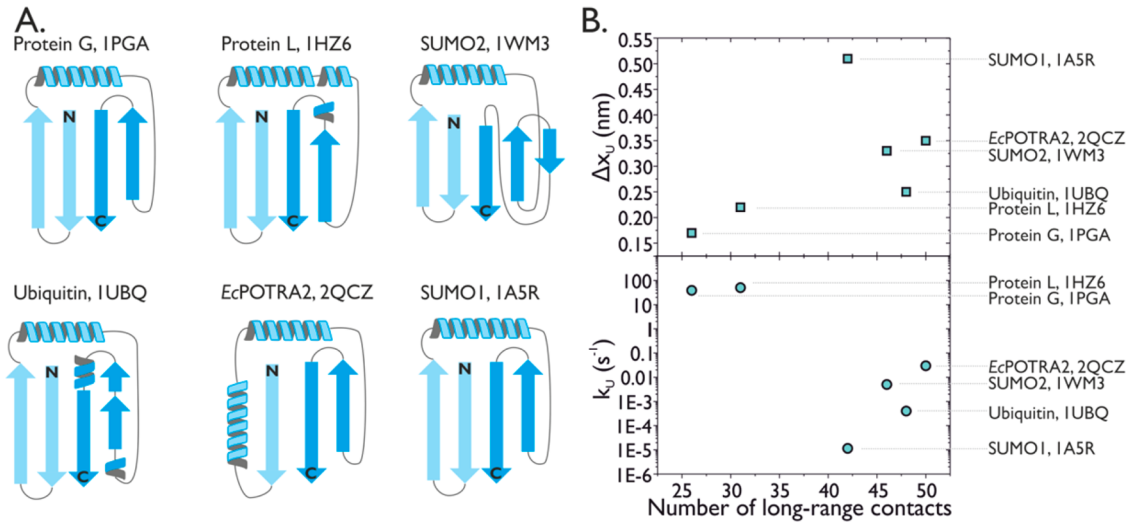

Figure 7. Two mechanical sub-units are identified in each of the six $\alpha + \beta$ proteins, protein G, protein L, SUMO2, Ubiquitin, *Ec*POTRA2, and SUMO1. The units are shown in light blue and dark blue. (B) The number of interfacial contacts between the mechanical sub-units is obtained, using contact maps of side chains with a distance between atoms of two residues of <5 Å. The number of interfacial contacts in the six $\alpha + \beta$ proteins which have proximal terminal β-strands in parallel geometry are protein G (26), protein L (31), SUMO2 (46), Ubiquitin (48), *Ec*POTRA2 (50), and SUMO1 (42). The number of interfacial contacts is shown against Δx_U (upper) and k_U (lower).

bonds between N- and C-terminal β-strands in the six $\alpha + \beta$ proteins that have proximal terminal β-strands in parallel geometry and found that it did not correlate with Δx_U or k_U (Figure S5). Therefore, the best correlation we have identified for these six $\alpha + \beta$ proteins is that between the total number of inter-residue contacts and Δx_U (Figure 6B, upper) and k_U (Figure 6B, lower).

This suggests that other features of the protein structure must be responsible for tailoring their mechanical properties. By fine-tuning our understanding of protein stability and malleability we obtain more robust predictive tools for understanding the mechanical properties of previously mechanically uncharacterized proteins. Such insight will be increasingly important for the rational design of novel, protein-based materials.

CONCLUSIONS

We have successfully demonstrated that GA cloning can be used to rapidly produce chimeric polyprotein sequences for use in AFM-based force spectroscopy. We designed new linker peptides (Figure 2) to allow for an ordered assembly of DNA fragments (Figure 1). These novel linker peptides did not affect the observed mechanical properties of *Tm*Csp and I27 compared to a previously characterized polyprotein that only differed in its linker sequences (Figures S1 and S2 and Supporting Information for linker sequences). Most importantly, this cloning method is able to significantly reduce the time required to obtain protein samples. The ability to assemble polyproteins from a set of premade DNA building blocks will increase the design flexibility for the generation of future constructs. It is also feasible to combine constructs by subsequent assembly reactions. This would allow the generation of longer polyproteins (*e.g.*, $(X\text{-}Y)_6$-I27 or $(X\text{-}Y)_3$-$(U\text{-}W)_3$-I27) that would otherwise be too labor- and time-intensive to produce. It is our hope that the application of GA cloning to the production of polyproteins will contribute to increasing the number of protein domains that will be mechanically studied in single-molecule experiments. Thus, it will help to broaden our understanding of the forces that define the folding and topologies of amino acid chains. Moreover, this technique enables the generation of previously impracticable constructs, increasing the variety of possible experimental setups.

Using this method we generated a chimeric polyprotein containing the previously unstudied *Ec*POTRA2 domain (Figure 3). We show that *Ec*POTRA2 is mechanically robust and that it is a suitable domain for force spectroscopy studies (Figure 4). By comparing the structure of *Ec*POTRA2 with other $\alpha + \beta$ proteins (Figure 5) studied using single-molecule AFM, we find a similar structural feature, namely, terminal β-strands which are proximal in a parallel geometry. For this subset of proteins we identify a clear correlation between their mechanical robustness and brittleness and the number of inter-residue contacts (Figure 6).

METHODS

Polyprotein Construction by Gibson Assembly. Specific primers were used to amplify six DNA cassettes by the polymerase chain reaction that encode individual protein domains as well as the linearized backbone (a modified pET8c vector[58] containing the N-terminal I27 domain (Table 1, Supporting Information)).

This step added the cassette-specific ends (which encode the amino acid sequence of the linkers) to enable an ordered assembly reaction (Figure 1). PCR products were purified by gel extraction (Qiagen gel extraction kit, UK). The six purified PCR-amplified DNA cassettes plus the vector backbone were joined to form a circular DNA molecule by GA cloning following the manufacturer's (NEB, MA, USA) instructions, using 100 ng of linearized vector backbone and a 5-fold molar excess of inserts. The reaction was incubated for 1 h at 50 °C in a thermocycler (PTC-100, MJ Research Inc., MA, USA), and 1 μL of the reaction mix was subsequently used to transform 25 μL of NEB 5-alpha competent *E. coli* cells. DNA plasmids encoding full-length assembled constructs were identified by colony PCR using T7 promoter (5′-TAATACGACTCACTATAGGG-3′) and T7 terminator (5′-GCTAGTTATTGCTCAGCGG-3′) primers, and their sequences were verified (Beckman Coulter Genomics, Takeley, UK).

Protein Expression and Purification. The polyprotein-encoding expression vector was transformed into *E. coli* BLR [DE3] pLysS (Novagen, Nottingham, UK). A 100 mL overnight starter culture (LB medium) was used to inoculate 10 × 1 L of LB medium supplemented with 25 μg mL^{-1} chloramphenicol and 100 μg mL^{-1} carbenicillin to obtain a starting optical density at 600 nm (OD_{600}) of 0.05. Culture incubation was carried out at 37 °C in an incubator shaker. At an OD_{600} = 0.5−0.6 protein expression was induced with 1 mM (final concentration) isopropyl β-D-thiogalactopyranoside (IPTG). Three hours later the cells were harvested by centrifugation. The cell pellet was resuspended in lysis buffer (20 mM Tris, 300 mM NaCl, 0.025% (w/v) sodium azide, 0.15% (v/v) Triton X-100, 5 mM imidazole, pH 8), and the cells were mechanically disrupted under high flow pressure (TS series cell disrupter, Constant Systems Ltd., Warwick, UK). The hexahistidine-tagged polyprotein was isolated from the cleared lysate using a Ni-NTA affinity chromatography resin (Ni sepharose HP, GE Healthcare, Sweden). The eluted protein was dialyzed into distilled deionized water and freeze-dried. The protein was then purified to homogeneity by size-exclusion chromatography. Protein resuspended in 63 mM sodium phosphate, pH 7.4, was separated by application to a 320 mL HiLoad 26/60 Superdex 75 column (GE Healthcare, Sweden). Captured fractions containing purified polyprotein were pooled and dialyzed against distilled deionized water before being aliquoted and stored at −20 °C.

Single-Molecule Force Spectroscopy. Single-molecule force spectroscopy experiments were completed for the chimeric polyproteins (I27-*Tm*Csp)$_3$-I27^{GA} and (I27-*Ec*POTRA2)$_3$-I27 using a method described previously.[35] Briefly, a custom-built AFM was mounted with silicon nitride cantilevers (MLCT, Veeco, Santa Barbara, CA, USA). The spring constant of the cantilever was found in buffer by applying the equipartition theorem[61] and was typically found to be 35 ± 3 pN nm^{-1}. A freeze-dried protein sample (0.1 mg) was reconstituted to 0.5 mg mL^{-1} in sterile sodium phosphate buffer (63 mM, pH 7.4) and centrifuged for 5 min at 14500*g* (Espresso personal microcentrifuge, Thermo Scientific, UK). Forty μL of the protein solution was applied onto a coverslip with a freshly stripped gold surface, which resulted in the immobilization of polyproteins *via* covalent attachment between the sulfydryl groups of two cysteine residues at the C-terminus of the polyprotein and the gold surface. After incubation for 15 min, the surface was rinsed with buffer. Mechanical unfolding experiments were performed at pulling velocities of 100, 200, 600, and 2000 nm s^{-1} at room temperature (23 °C) over a distance of 400 nm. Three data sets, each containing at least 28 unfolding events for the domain under study (*Tm*Csp or *Ec*POTRA2), were accumulated at each pulling velocity using a fresh sample and a new cantilever for each data set.

Analysis of Single-Molecule Force−Extension Data. Data from single-molecule force−extension experiments for the chimeric polyproteins were filtered to include only traces that show the unfolding of a single polyprotein chain. This is characterized by displaying seven or fewer unfolding events. The spectra were subsequently analyzed using in-house software written for IGOR Pro (version 6, Wavemetrics, Lake Oswego, OR, USA). Initially, a model-free analysis was carried out. Here, the peak unfolding force of each protein unfolding event and the interpeak distance between unfolding events (x_{p2p}), defined as the distance between one peak and the same force value on the following sawtooth curve, were recorded. The unfolding forces and interpeak distances were binned and plotted in histograms, allowing Gaussian plots of the data to be obtained. To obtain an estimate of the number of amino acids that are released from a compact, globular native state to an extended state during each unfolding event, the data were analyzed by fitting a worm-like-chain (WLC) model for polymer elasticity[62] to the rising edge of each sawtooth, as described previously.[63] The WLC model is given by

$$F(x) = \frac{k_B T}{p}\left(\frac{1}{4\left(1-\frac{x}{L_C}\right)^2} - \frac{1}{4} + \frac{x}{L_C}\right)$$

where $F(x)$ is the force as a function of extension, x; k_B is Boltzmann's constant, p is the persistence length, and L_C is the contour length.

Monte Carlo (MC) Simulations. MC simulations were performed using a two-state model for unfolding, as described previously.[34,35] This technique is based on the assumption that each protein unfolds *via* a two-state all-or-none process governed by a rate constant, k_U, and the distance from the native state to the transition state along the measured reaction coordinate, Δx_U. The simulations were used to generate histograms of unfolding forces for protein domains at a particular pulling velocity and compared to those generated experimentally. The pair of k_U and Δx_U values that provided the best global fit to the experimental data over all pulling velocities was obtained. The uncertainty in the experimental data, defined as the standard error in the straight line fit to the dependence of F_U on the pulling speed, was used to quantify the uncertainty in k_U and Δx_U. The range of k_U and Δx_U values that provided a fit to the data within the experimental uncertainty gave the value of the uncertainty for each parameter.

Conflict of Interest: The authors declare no competing financial interest.

Supporting Information Available: The Supporting Information is available free of charge on the ACS Publications website at DOI: 10.1021/acsnano.5b01962.

Further details of primers used for the GA method as well as the single-molecule protein unfolding experiments, including unfolding force histograms and tables with the number of events for each experiment and a comparison of the pulling speed dependence of the I27 protein in the three different polyprotein constructs (PDF)

Acknowledgment. L.D. is supported by a grant from the European Research Council (258259-EXTREME BIOPHYSICS). B.S. is funded by a White Rose DTP BBSRC studentship. We would like to thank members of the Dougan and Brockwell groups for useful discussions and feedback.

REFERENCES AND NOTES

1. Borgia, A.; Williams, P. M.; Clarke, J. Single-Molecule Studies of Protein Folding. *Annu. Rev. Biochem.* **2008**, *77*, 101–125.
2. Galera-Prat, A.; Gómez-Sicilia, A.; Oberhauser, A. F.; Cieplak, M.; Carrión-Vázquez, M. Understanding Biology by Stretching Proteins: Recent Progress. *Curr. Opin. Struct. Biol.* **2010**, *20*, 63–9.
3. Hoffmann, T.; Dougan, L. Single Molecule Force Spectroscopy Using Polyproteins. *Chem. Soc. Rev.* **2012**, *41*, 4781–4796.
4. Marszalek, P. E.; Dufrene, Y. F. Stretching Single Polysaccharides and Proteins Using Atomic Force Microscopy. *Chem. Soc. Rev.* **2012**, *41*, 3523–3534.
5. Rief, M.; Gautel, M.; Oesterhelt, F.; Fernandez, J. M.; Gaub, H. E. Reversible Unfolding of Individual Titin Immunoglobulin Domains by AFM. *Science* **1997**, *276*, 1109–1112.
6. Zoldak, G.; Rief, M. Force as a Single Molecule Probe of Multidimensional Protein Energy Landscapes. *Curr. Opin. Struct. Biol.* **2013**, *23*, 48–57.

7. Tych, K. M.; Hoffmann, T.; Batchelor, M.; Hughes, M. L.; Kendrick, K. E.; Walsh, D. L.; Wilson, M.; Brockwell, D. J.; Dougan, L. Life in extreme environments: single molecule force spectroscopy as a tool to explore proteins from extremophilic organisms. *Biochem. Soc. Trans.* **2015**, *43*, 179–185.
8. Garcia-Manyes, S.; Brujic, J.; Badilla, C. L.; Fernandez, J. M. Force-Clamp Spectroscopy of Single-Protein Monomers Reveals the Individual Unfolding and Folding Pathways of I27 and Ubiquitin. *Biophys. J.* **2007**, *93*, 2436–2446.
9. Aggarwal, V.; Kulothungan, S. R.; Rajaram, S.; Balamurali, M. M.; Varadarajan, R.; Ainavarapu, S. R. K. Single-Molecule Studies of the Parallel Unfolding Pathways of Maltose Binding Protein (MBP). *Biophys. J.* **2011**, *100*, 481–481.
10. Carrion-Vazquez, M.; Oberhauser, A. F.; Fowler, S. B.; Marszalek, P. E.; Broedel, S. E.; Clarke, J.; Fernandez, J. M. Mechanical and Chemical Unfolding of a Single Protein: A Comparison. *Proc. Natl. Acad. Sci. U. S. A.* **1999**, *96*, 3694–3699.
11. Steward, A.; Toca-Herrera, J. L.; Clarke, J. Versatile Cloning System for Construction of Multimeric Proteins for Use in Atomic Force Microscopy. *Protein Sci.* **2002**, *11*, 2179–2183.
12. Hoffmann, T.; Tych, K. M.; Hughes, M. L.; Brockwell, D. J.; Dougan, L. Towards Design Principles for Determining the Mechanical Stability of Proteins. *Phys. Chem. Chem. Phys.* **2013**, *15*, 15767–15780.
13. Berkemeier, F.; Bertz, M.; Xiao, S. B.; Pinotsis, N.; Wilmanns, M.; Grater, F.; Rief, M. Fast-Folding Alpha-Helices as Reversible Strain Absorbers in the Muscle Protein Myomesin. *Proc. Natl. Acad. Sci. U. S. A.* **2011**, *108*, 14139–14144.
14. Cao, Y.; Lam, C.; Wang, M. J.; Li, H. B. Nonmechanical Protein Can Have Significant Mechanical Stability. *Angew. Chem., Int. Ed.* **2006**, *45*, 642–645.
15. Gao, X.; Qin, M.; Yin, P. G.; Liang, J. Y.; Wang, J.; Cao, Y.; Wang, W. Single-Molecule Experiments Reveal the Flexibility of a Per-ARNT-Sim Domain and the Kinetic Partitioning in the Unfolding Pathway under Force. *Biophys. J.* **2012**, *102*, 2149–2157.
16. Sharma, D.; Perisic, O.; Peng, Q.; Cao, Y.; Lam, C.; Lu, H.; Li, H. B. Single-Molecule Force Spectroscopy Reveals a Mechanically Stable Protein Fold and the Rational Tuning of its Mechanical Stability. *Proc. Natl. Acad. Sci. U. S. A.* **2007**, *104*, 9278–9283.
17. Bertz, M.; Rief, M. Mechanical Unfoldons as Building Blocks of Maltose-Binding Protein. *J. Mol. Biol.* **2008**, *378*, 447–458.
18. Bertz, M.; Rief, M. Ligand Binding Mechanics of Maltose Binding Protein. *J. Mol. Biol.* **2009**, *393*, 1097–1105.
19. Dietz, H.; Bertz, M.; Schlierf, M.; Berkemeier, F.; Bornschlogl, T.; Junker, J. P.; Rief, M. Cysteine Engineering of Polyproteins for Single-Molecule Force Spectroscopy. *Nat. Protoc.* **2006**, *1*, 80–84.
20. Dietz, H.; Rief, M. Protein Structure by Mechanical Triangulation. *Proc. Natl. Acad. Sci. U. S. A.* **2006**, *103*, 1244–1247.
21. Guzmán, D. L.; Randall, A.; Baldi, P.; Guan, Z. Computational and Single-Molecule Force Studies of a Macro Domain Protein Reveal a Key Molecular Determinant for Mechanical Stability. *Proc. Natl. Acad. Sci. U. S. A.* **2010**, *107*, 1989–94.
22. Yang, G.; Cecconi, C.; Baase, W. A.; Vetter, I. R.; Breyer, W. A.; Haack, J. A.; Matthews, B. W.; Dahlquist, F. W.; Bustamante, C. Solid-State Synthesis and Mechanical Unfolding of Polymers of T4 Lysozyme. *Proc. Natl. Acad. Sci. U. S. A.* **2000**, *97*, 139–144.
23. Zhao, J. M.; Lee, H.; Nome, R. A.; Majid, S.; Scherer, N. F.; Hoff, W. D. Single-Molecule Detection of Structural Changes During Per-Arnt-Sim (PAS) Domain Activation. *Proc. Natl. Acad. Sci. U. S. A.* **2006**, *103*, 11561–11566.
24. Zheng, P.; Chou, C. C.; Guo, Y.; Wang, Y. Y.; Li, H. B. Single Molecule Force Spectroscopy Reveals the Molecular Mechanical Anisotropy of the FeS4Metal Center in Rubredoxin. *J. Am. Chem. Soc.* **2013**, *135*, 17783–17792.
25. Zheng, P.; Takayama, S. I. J.; Mauk, A. G.; Li, H. B. Hydrogen Bond Strength Modulates the Mechanical Strength of Ferric-Thiolate Bonds in Rubredoxin. *J. Am. Chem. Soc.* **2012**, *134*, 4124–4131.
26. Zheng, P.; Takayama, S. J.; Mauk, A. G.; Li, H. B. Single Molecule Force Spectroscopy Reveals That Iron Is Released from the Active Site of Rubredoxin by a Stochastic Mechanism. *J. Am. Chem. Soc.* **2013**, *135*, 7992–8000.
27. Zheng, P.; Cao, Y.; Li, H. Facile Method of Constructing Polyproteins for Single-Molecule Force Spectroscopy Studies. *Langmuir* **2011**, *27*, 5713–8.
28. Bornschlogl, T.; Rief, M. Single-Molecule Dynamics of Mechanical Coiled-Coil Unzipping. *Langmuir* **2008**, *24*, 1338–1342.
29. Dietz, H.; Rief, M. Exploring the Energy Landscape of GFP by Single-Molecule Mechanical Experiments. *Proc. Natl. Acad. Sci. U. S. A.* **2004**, *101*, 16192–7.
30. Hermans, R. I. Probability of Observing a Number of Unfolding Events while Stretching Polyproteins. *Langmuir* **2014**, *30*, 8650–8655.
31. Zinober, R. C.; Brockwell, D. J.; Beddard, G. S.; Blake, A. W.; Olmsted, P. D.; Radford, S. E.; Smith, D. A. Mechanically Unfolding Proteins: The Effect of Unfolding History and the Supramolecular Scaffold. *Protein Sci.* **2002**, *11*, 2759–2765.
32. Tych, K. M.; Hughes, M. L.; Bourke, J.; Taniguchi, Y.; Kawakami, M.; Brockwell, D. J.; Dougan, L. Optimizing the calculation of energy landscape parameters from single-molecule protein unfolding experiments. *Phys. Rev. E* **2015**, *91*, 91.
33. Gibson, D. G.; Young, L.; Chuang, R. Y.; Venter, J. C.; Hutchison, C. A.; Smith, H. O. Enzymatic Assembly of DNA Molecules Up to Several Hundred Kilobases. *Nat. Methods* **2009**, *6*, 343–U41.
34. Hoffmann, T.; Tych, K. M.; Brockwell, D. J.; Dougan, L. Single-Molecule Force Spectroscopy Identifies a Small Cold Shock Protein as Being Mechanically Robust. *J. Phys. Chem. B* **2013**, *117*, 1819–1826.
35. Tych, K. M.; Hoffmann, T.; Brockwell, D. J.; Dougan, L. Single Molecule Force Spectroscopy Reveals the Temperature-Dependent Robustness and Malleability of a Hyperthermophilic Protein. *Soft Matter* **2013**, *9*, 9016–9025.
36. Kim, S.; Malinverni, J. C.; Sliz, P.; Silhavy, T. J.; Harrison, S. C.; Kahne, D. Structure and Function of an Essential Component of the Outer Membrane Protein Assembly Machine. *Science* **2007**, *317*, 961–964.
37. Kim, K. H.; Aulakh, S.; Paetzel, M. The Bacterial Outer Membrane β-Barrel Assembly Machinery. *Protein Sci.* **2012**, *21*, 751–768.
38. Clantin, B.; Delattre, A. S.; Rucktooa, P.; Saint, N.; Meli, A. C.; Locht, C.; Jacob-Dubuisson, F.; Villeret, V. Structure of the Membrane Protein FhaC: A Member of the Omp85-TpsB Transporter Superfamily. *Science* **2007**, *317*, 957–961.
39. Gentle, I. E.; Burri, L.; Lithgow, T. Molecular Architecture and Function of the Omp85 Family of Proteins. *Mol. Microbiol.* **2005**, *58*, 1216–1225.
40. Sanchez-Pulido, L.; Devos, D.; Genevrois, S.; Vicente, M.; Valencia, A. POTRA: a Conserved Domain in the FtsQ Family and a Class of Beta-Barrel Outer Membrane Proteins. *Trends Biochem. Sci.* **2003**, *28*, 523–526.
41. Gatzeva-Topalova, P. Z.; Walton, T. A.; Sousa, M. C. Crystal Structure of YaeT: Conformational Flexibility and Substrate Recognition. *Structure* **2008**, *16*, 1873–1881.
42. Sinnige, T.; Weingarth, M.; Renault, M.; Baker, L.; Tommassen, J.; Baldus, M. Solid-State NMR Studies of Full-Length BamA in Lipid Bilayers Suggest Limited Overall POTRA Mobility. *J. Mol. Biol.* **2014**, *426*, 2009–2021.
43. Chen, Y.; Radford, S. E.; Brockwell, D. J. Force-Induced Remodelling of Proteins and Their Complexes. *Curr. Opin. Struct. Biol.* **2015**, *30*, 89–99.
44. Farrance, O. E.; Hann, E.; Kaminska, R.; Housden, N. G.; Derrington, S. R.; Kleanthous, C.; Radford, S. E.; Brockwell, D. J. A Force-Activated Trip Switch Triggers Rapid Dissociation of a Colicin from Its Immunity Protein. *PLoS Biol.* **2013**, *11*, 11.
45. Knowles, T. J.; Jeeves, M.; Bobat, S.; Dancea, F.; McClelland, D.; Palmer, T.; Overduin, M.; Henderson, I. R. Fold and

Function of Polypeptide Transport-Associated Domains Responsible for Delivering Unfolded Proteins to Membranes. *Mol. Microbiol.* **2008**, *68*, 1216–1227.
46. Lu, H.; Schulten, K. The Key Event in Force-Induced Unfolding of Titin's Immunoglobulin Domains. *Biophys. J.* **2000**, *79*, 51–65.
47. Sikora, M.; Sulkowska, J. I.; Witkowski, B. S.; Cieplak, M. BSDB: the Biomolecule Stretching Database. *Nucleic Acids Res.* **2011**, *39*, D443–50.
48. Li, M. S.; Klimov, D. K.; Thirumalai, D. Thermal Denaturation and Folding Rates of Single Domain Proteins: Size Matters. *Polymer* **2004**, *45*, 573–579.
49. Arad-Haase, G.; Chuartzman, S. G.; Dagan, S.; Nevo, R.; Kouza, M.; Mai, B. K.; Nguyen, H. T.; Li, M. S.; Reich, Z. Mechanical Unfolding of Acylphosphatase Studied by Single-Molecule Force Spectroscopy and MD Simulations. *Biophys. J.* **2010**, *99*, 238–247.
50. Best, R. B.; Li, B.; Steward, A.; Daggett, V.; Clarke, J. Can Non-Mechanical Proteins Withstand Force? Stretching Barnase by Atomic Force Microscopy and Molecular Dynamics Simulation. *Biophys. J.* **2001**, *81*, 2344–2356.
51. Brockwell, D. J.; Beddard, G. S.; Paci, E.; West, D. K.; Olmsted, P. D.; Smith, D. A.; Radford, S. E. Mechanically Unfolding the Small, Topologically Simple Protein L. *Biophys. J.* **2005**, *89*, 506–519.
52. Cao, Y.; Li, H. Polyprotein of GB1 is an Ideal Artificial Elastomeric Protein. *Nat. Mater.* **2007**, *6*, 109–114.
53. Carrion-Vazquez, M.; Li, H. B.; Lu, H.; Marszalek, P. E.; Oberhauser, A. F.; Fernandez, J. M. The Mechanical Stability of Ubiquitin is Linkage Dependent. *Nat. Struct. Biol.* **2003**, *10*, 738–743.
54. Cecconi, C.; Shank, E. A.; Bustamante, C.; Marqusee, S. Direct Observation of the Three-State Folding of a Single Protein Molecule. *Science* **2005**, *309*, 2057–2060.
55. Gao, X.; Qin, M.; Yin, P.; Liang, J.; Wang, J.; Cao, Y.; Wang, W. Single-Molecule Experiments Reveal the Flexibility of a Per-ARNT-Sim Domain and the Kinetic Partitioning in the Unfolding Pathway under Force. *Biophys. J.* **2012**, *102*, 2149–2157.
56. He, C.; Genchev, G. Z.; Lu, H.; Li, H. Mechanically Untying a Protein Slipknot: Multiple Pathways Revealed by Force Spectroscopy and Steered Molecular Dynamics Simulations. *J. Am. Chem. Soc.* **2012**, *134*, 10428–10435.
57. Kotamarthi, H. C.; Sharma, R.; Ainavarapu, R. K. Single-Molecule Studies on PolySUMO Proteins Reveal Their Mechanical Flexibility. *Biophys. J.* **2013**, *104*, 2273–2281.
58. Brockwell, D. J.; Beddard, G. S.; Clarkson, J.; Zinober, R. C.; Blake, A. W.; Trinick, J.; Olmsted, P. D.; Smith, D. A.; Radford, S. E. The Effect of Core Destabilization on the Mechanical Resistance of I27. *Biophys. J.* **2002**, *83*, 458–472.
59. Kolmakov, G. V.; Matyjaszewski, K.; Balazs, A. C. Harnessing Labile Bonds between Nanogel Particles to Create Self-Healing Materials. *ACS Nano* **2009**, *3*, 885–892.
60. Vehlow, C.; Stehr, H.; Winkelmann, M.; Duarte, J. M.; Petzold, L.; Dinse, J.; Lappe, M. CMView: Interactive Contact Map Visualization and Analysis. *Bioinformatics* **2011**, *27*, 1573–1574.
61. Florin, E. L.; Rief, M.; Lehmann, H.; Ludwig, M.; Dornmair, C.; Moy, V. T.; Gaub, H. E. Sensing Specific Molecular-Interactions with the Atomic-Force Microscope. *Biosens. Bioelectron.* **1995**, *10*, 895–901.
62. Marko, J. F.; Siggia, E. D. Stretching DNA. *Macromolecules* **1995**, *28*, 8759–8770.
63. Bustamante, C.; Marko, J. F.; Siggia, E. D.; Smith, S. Entropic Elasticity of Lambda-Phage DNA. *Science* **1994**, *265*, 1599–1600.